High resolution microscopy reveals an unusual architecture of the *Plasmodium berghei* endoplasmic reticulum

Gesine Kaiser,[1,2] Mariana De Niz,[1,4] Benoît Zuber,[3] Paul-Christian Burda,[1] Benoît Kornmann,[5] Volker T. Heussler[1†] and Rebecca R. Stanway[1*†]

[1] Institute of Cell Biology, University of Bern, Baltzerstr. 4, 3012 Bern, Switzerland, [2] Graduate School for Cellular and Biomedical Sciences,
[3] Institute of Anatomy, University of Bern, Baltzerstrasse 2, 3012, Bern, Switzerland.
[4] Wellcome Trust Center for Molecular Parasitology, G12 8TA, Glasgow, UK.
[5] Institute of Biochemistry, ETH Zürich, Otto-Stern-Weg 3, 8093, Zürich, Switzerland.

Summary

To fuel the tremendously fast replication of *Plasmodium* liver stage parasites, the endoplasmic reticulum (ER) must play a critical role as a major site of protein and lipid biosynthesis. In this study, we analysed the parasite's ER morphology and function. Previous studies exploring the parasite ER have mainly focused on the blood stage. Visualizing the *Plasmodium berghei* ER during liver stage development, we found that the ER forms an interconnected network throughout the parasite with perinuclear and peripheral localizations. Surprisingly, we observed that the ER additionally generates huge accumulations. Using stimulated emission depletion microscopy and serial block-face scanning electron microscopy, we defined ER accumulations as intricate dense networks of ER tubules. We provide evidence that these accumulations are functional subdivisions of the parasite ER, presumably generated in response to elevated demands of the parasite, potentially consistent with ER stress. Compared to higher eukaryotes, *Plasmodium* parasites have a fundamentally reduced unfolded protein response machinery for reacting to ER stress. Accordingly, parasite development is greatly impaired when ER stress is applied. As parasites appear to be more sensitive to ER stress than are host cells, induction of

Accepted 24 August, 2016. *For correspondence. E-mail rebecca.limenitakis@izb.unibe.ch; Tel. +41 316314673; Fax +41 316314431.
[†]These authors contributed equally to the work.

ER stress could potentially be used for interference with parasite development.

Introduction

Plasmodium parasites are transmitted by the bite of an infected female *Anopheles* mosquito, which injects a moderate number of sporozoites into its host (about 100 in the case of *P. berghei*) (Frischknecht *et al.*, 2004). About a third of the injected sporozoites find a blood vessel and travel through the bloodstream until they reach the liver. Here they invade and infect hepatocytes, thereby forming a parasitophorous vacuole membrane (PVM) (Bano *et al.*, 2007). Within the parasitophorous vacuole (PV), parasites undergo extensive replication by schizogony; a single sporozoite can differentiate into up to 30,000 merozoites, depending on the species (Menard *et al.*, 2013). In parallel with nuclear replication, the parasite has to expand its other vital organelles and ultimately provide sufficient membranous material to surround single daughter parasites (Sturm *et al.*, 2009; Stanway *et al.*, 2011). *Plasmodium* replication and growth, particularly in the liver, are very fast and resource-demanding processes. Despite the scavenging of host lipids and nutrients, the parasite must still produce enormous amounts of protein and lipid within minimal time (Mikolajczak *et al.*, 2007; Blume *et al.*, 2011; Slavic *et al.*, 2011; Itoe *et al.*, 2014). In addition to specialized organelles like micronemes, rhoptries and dense granules, *Plasmodium* possesses a rather classical set of secretory organelles, such as an ER and a single Golgi apparatus (Striepen *et al.*, 2007). So far, description of their morphology and biogenesis is rudimental and restricted to *Plasmodium* blood stage parasites (van Dooren *et al.*, 2005; Struck *et al.*, 2005, 2008b).

The ER is an essential organelle in eukaryotic cells. It typically makes up almost half of the cell's membranous material and is crucial for lipid biosynthesis, protein folding, calcium storage and protein secretion. Interestingly, the architecture of the ER has been recently described to have a greater influence on its function than pzreviously anticipated (Westrate *et al.*, 2015). ER sheets, or cisternae, are often found in a stacked conformation, coated with ribosomes, their main function being protein synthesis, folding, and post-translational modification.
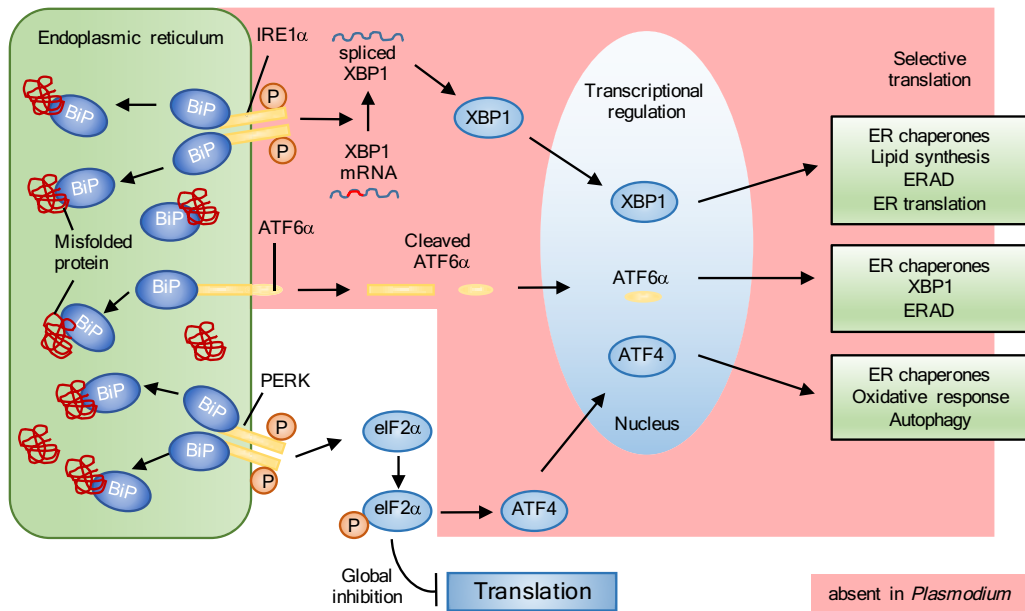
Fig. 1. *Plasmodium* parasites possess a greatly reduced unfolded protein response (UPR) machinery compared to higher eukaryotes. So far, only homologues of the chaperone BiP, the ER stress sensor PERK and the downstream component eIF2α have been identified in *Plasmodium* parasites. Accordingly, parasites are only able to react to ER stress by inhibition of global translation and are devoid of selective transcriptional regulation. UPR components not identified in *Plasmodium* have a red background, components identified have a white background (adapted from Gosline *et al.*, 2011; Harbut *et al.*, 2012; Janssens *et al.*, 2014; Wang and Kaufman, 2014).

ER tubules are generally organized in dynamic, constantly rearranging and extending networks that function primarily in lipid biosynthesis. The ER can form direct contact with other membranes at membrane contact sites (MCS) (Phillips and Voeltz, 2015). In yeast such contacts occur, for example, with the mitochondrion, where they are important for lipid biosynthesis and calcium signalling (Kornmann and Walter, 2010).

Major components of membranes, such as phospholipids and proteins, are sorted within the ER and transferred to specialized regions called ER-Golgi intermediate compartments (ERGICs), which are in close proximity to the Golgi apparatus. Cargo from the ER is packed into COPII-coated vesicles and leaves the ER at distinct, long-lived transitional ER (tER) sites, also called ER exit sites (Szul and Sztul, 2011). It is proposed that secretory material first passes through the ERGIC before fusing with the cis-Golgi (Hammond and Glick, 2000). It has been suggested that *P. falciparum* parasites possess the machinery for COPII-coated vesicle transport as parasites encode components of this machinery and have distinct tER sites that are closely juxtaposed to the cis-Golgi, following the dynamics of the cis-Golgi (Struck *et al.*, 2008b). The *Plasmodium* ER has been proposed to make contacts with the inner membrane complex (Hanssen *et al.*, 2013), but whether the *Plasmodium* ER forms contacts with other organelles or the plasma membrane (PM), and whether proteins are transported through an ERGIC has not been described.

High demands for protein synthesis will cause overloading of the ER with unfolded and misfolded proteins, as space and chaperone numbers become restricted, which leads to an increased error rate in protein folding. If too many unfolded or misfolded proteins are present in the ER, an ER stress response known as the unfolded protein response (UPR) is mounted, which seeks to restore ER homeostasis (Wu *et al.*, 2014). Apicomplexan parasites appear to harbour a dramatically reduced UPR machinery, with only Binding immunoglobulin Protein (BiP) and PERK homologues identified in the genome. If this is true, *Plasmodium* parasites would only be able to globally downregulate translation upon ER stress but would lack the transcriptionally mediated UPR (Gosline *et al.*, 2011; Joyce *et al.*, 2013) (Fig. 1).

In this study, we have analysed by microscopy the morphology and biogenesis of the ER in *Plasmodium berghei* parasites, with a focus on the liver stage, using transgenic parasite lines expressing fluorescently tagged marker proteins for the ER, tER, cis- and trans-Golgi faces. We found that the *Plasmodium* ER forms extensive accumulations during asexual replication. Utilizing serial block-face scanning electron microscopy (SBFSEM), we were able to define these accumulations as voluminous, intricate and dense networks of ER tubules. We hypothesize that these accumulations might allow the parasite ER to cope with the enormous protein throughput, and hence ER stress, to enable fast and massive parasite replication. Additionally, we found evidence that the parasite ER forms contact sites

with the PM or PVM and we speculate that these contact sites could allow nonvesicular lipid transfer to feed lipids into these rapidly expanding membranes.

Results

### *The endoplasmic reticulum of* P. berghei *liver stage parasites has an unusual architecture*

To visualize the parasite ER, we N-terminally tagged the *P. berghei* homologue of a well described ER marker protein, PbSec61β, with both GFP and superfolder GFP (sfGFP) (Couffin *et al.*, 1998; Pédelacq *et al.*, 2006; Kornmann *et al.*, 2011). The sfGFP offers several advantages over GFP for the tagging of ER transmembrane proteins such as Sec61β. GFP has the tendency to weakly dimerize. When this occurs at the cytoplasmic face of the ER membrane, it can induce artificial reorganization of the entire ER architecture, resulting in huge ER patches known as organized smooth ER (Snapp *et al.*, 2003). In contrast, sfGFP is a purely monomeric version of GFP that was designed to exhibit improved folding capacities and to be more resistant to denaturation (Costantini and Snapp, 2013). We did not observe differences in the localization of the two fusion proteins and thus used both for our experiments. Transgenic parasites were generated, expressing either a GFP-PbSec61β or a sfGFP-PbSec61β fusion protein under the control of the constitutive *eef1αa* promoter, which allowed visualization of the ER throughout the parasite's life cycle (Fig. 2A). We focused on analysing the parasite ER during liver stage development, but for comparison also imaged other life cycle stages (Supporting Information Figs S1 and S2). Live cell imaging of Pb^{C}sfGFP-Sec61β parasites showed that during liver stage schizogony, the parasite ER closely surrounds each parasite nucleus and additionally builds a network of ER membranes that extend through the entire cytoplasm (Fig. 2B and Supporting Information Movie S1). The parasite ER seems to remain as a single interconnected organelle until very shortly before merozoite formation. In merozoites, only the perinuclear ER is present (Fig. 2B and Supporting Information Movie S1). To verify this observation, Pb^{C}GFP-Sec61β parasites were fixed towards the end of liver stage development, at 56 h post infection (hpi), and stained with an antiserum against PbMSP1 (merozoite surface protein 1, PBANKA_083100), which localizes to the parasite PM of late liver stage parasites. We were able to confirm by visualization of single daughter merozoites, defined by their surrounding PbMSP1-positive PM, that the ER is found mainly around the nucleus with occasional minor protrusions, but is not peripherally localized (Fig. 2C).

Surprisingly, we observed that the parasite ER, in addition to being perinuclear and existing as network-like structures, also forms extensive ER accumulations, which start to appear in trophozoites and become most prominent during the cytomere stage (Fig. 2B, red arrows). Measuring different focal planes of Pb^{C}sfGFP-Sec61β parasites ($n = 3$, 9 parasites per replicate; 5 random focal planes measured per parasite), these ER accumulations were estimated to account for about 24% of the total parasite area during the cytomere stage (Supporting Information Fig. S3). Interestingly, most of the ER accumulations disappear during the formation of individual merozoites and accumulations are completely absent at the end of liver stage development when merozoites have formed. To exclude that these ER accumulations are an artefact of GFP localization to the cytoplasmic face of ER membranes, we generated a specific antiserum against PbBiP, an ER chaperone localized in the ER lumen (Kumar *et al.*, 1991; Snapp *et al.*, 2003). We used this anti-PbBiP antiserum to stain HeLa cells infected with wild-type (WT) parasites (Fig. 3A) and Pb^{C}sfGFP-Sec61β parasites (Fig. 3B), both fixed at 48 hpi, which approximates to the cytomere stage. We observed ER accumulations in anti-PbBiP-stained WT parasites, which confirmed that ER accumulations occur naturally during parasite development. Co-localization of the anti-PbBiP staining with the sfGFP-Sec61β was examined by determining the Pearson's *R* value, which is 0.93, implying a high degree of co-localization. Importantly, we were also able to show by intravital microscopy that parasite ER accumulations are present *in vivo* in Pb^{C}sfGFP-Sec61β parasites at 42 hpi, and had disappeared in most parasites imaged at 49 hpi when merozoites had formed (Fig. 3C). This demonstrates that accumulations of parasite ER are indeed a natural feature of *P. berghei* development. We also found these ER accumulations in other phases of parasite replication (Supporting Information Figs S1 and S2). During blood stage schizogony, we observed ER accumulations from the ring stage onwards until they disappear in maturing schizonts. Blood stage merozoites seem to contain only the perinuclear ER, similar to liver stage merozoites. Interestingly, we also observed ER accumulations in gametocytes (Supporting Information Fig. S1). ER accumulations were also found during sporogony of the parasite in the mosquito midgut, but are absent in mature sporoblasts. Midgut and salivary gland sporozoites possess a perinuclear ER and a peripheral ER network, which spans through the entire sporozoite, but are devoid of ER accumulations (Supporting Information Figs S2 and S4). Together, it appears that ER accumulations are formed in proliferative parasite stages and are absent in non-proliferative stages.

High resolution microscopy offers insight into the nature of ER accumulations

When we examined ER accumulations using standard widefield fluorescence microscopy (FM), they appeared as

A

B

C
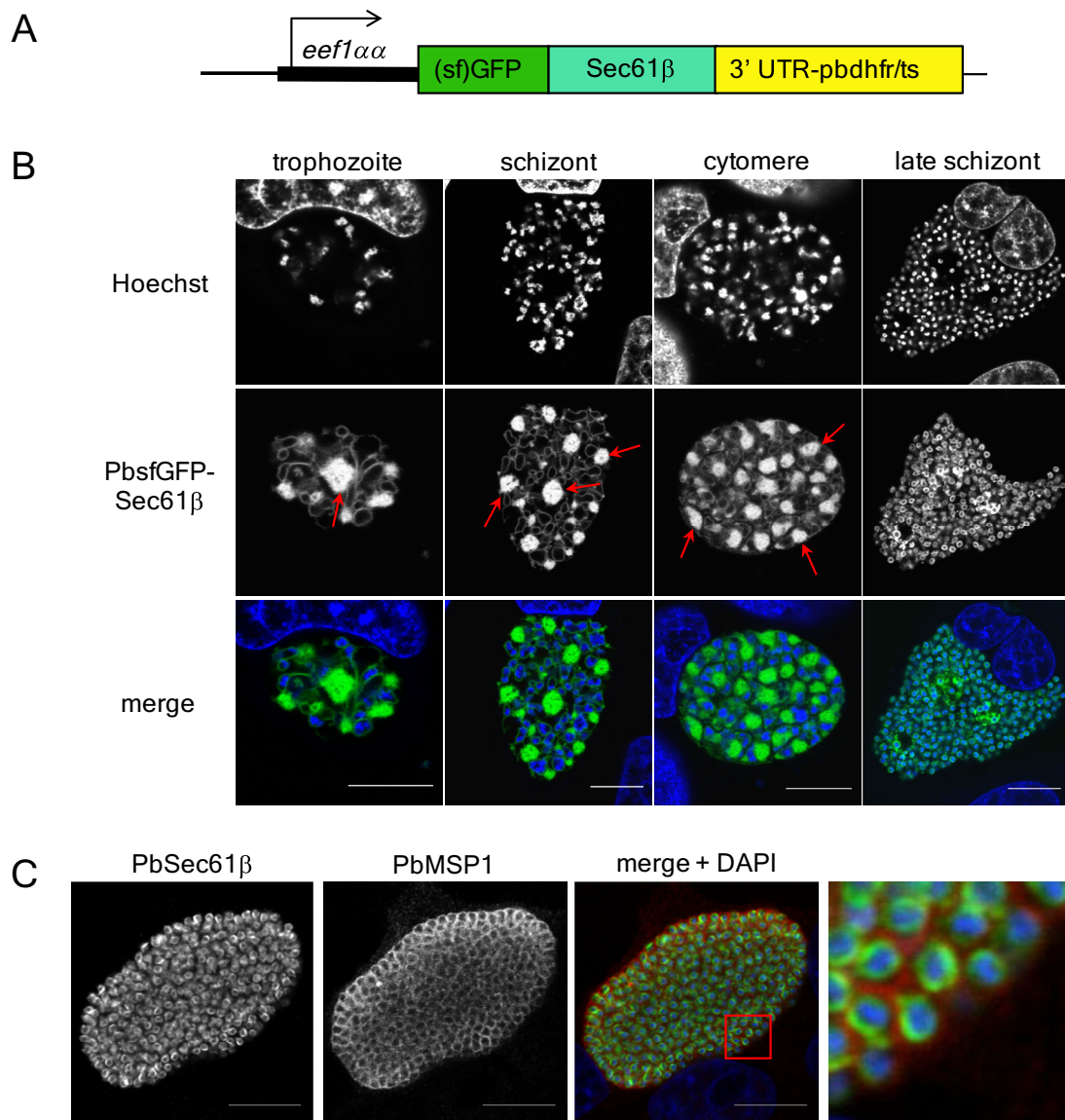
**Fig. 2.** Characterization of the *P. berghei* ER during liver stage development, visualized by expression of (sf)GFP-PbSec61β.
A. Schematic representation of the p^C(sf)GFP-PbSec61β plasmid. The fusion protein was expressed under the control of the constitutive *eef1αa* promoter and the 3′-UTR was taken from Pbdhfr/ts.
B. ER morphology of *Plasmodium* parasites during liver stage development. HeLa cells were infected with Pb^CsfGFP-Sec61β parasites (ER is shown in green) and monitored at different time points post infection by live cell confocal imaging. The *P. berghei* ER consists of a perinuclear ER and a peripheral ER network. Additionally, ER accumulations are formed during the trophozoite stage and disappear again once cytokinesis occurs. DNA (blue) was stained with Hoechst 33342. Red arrows point to ER accumulations.
C. The parasite ER divides upon cytokinesis and merozoite formation; only the perinuclear ER is inherited by daughter parasites. HeLa cells infected with Pb^CGFP-Sec61β parasites (green) were fixed at 56 hpi and stained with anti-PbMSP1 (red) and anti-GFP. DNA (blue) was visualized with DAPI. Area of the red box is displayed at a higher magnification. Scale bars correspond to 10 μm.

oval to round ER bodies, potentially formed through expansion of ER sheets or tubules (Fig. 4A). To unravel the architecture of ER accumulations in detail, we used stimulated emission depletion (STED) microscopy, which typically gives a resolution of 30–80 nm (Hell and Wichman, 1994). STED imaging of WT parasites fixed at 48 hpi and stained with anti-PbBiP antiserum, revealed that ER accumulations have a dense membranous tubular organization

(Fig. 4B). In order to resolve the structure of ER accumulations even further, we used electron microscopy (EM). Recently, there have been major advances in 3D EM using SBFSEM, which has been already used to look at morphological and volumetric changes of parasites in different blood stages of *P. falciparum* (Sakaguchi *et al.*, 2016). We used SBFSEM for imaging of FACS-sorted Pb^CmCherry parasites that were fixed at 48 hpi. By vertically cutting thin slices through our sample and subsequent imaging we
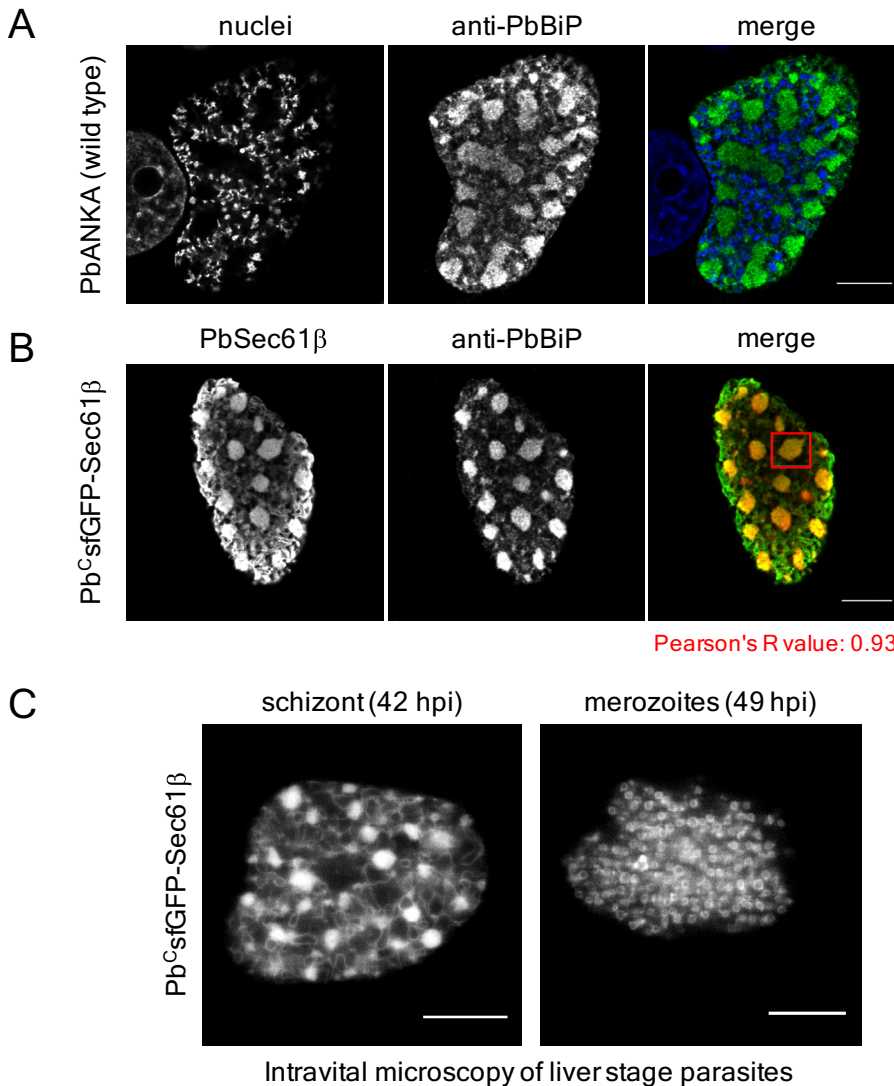
Fig. 3. ER accumulations occur naturally during *in vitro* and *in vivo* parasite development.
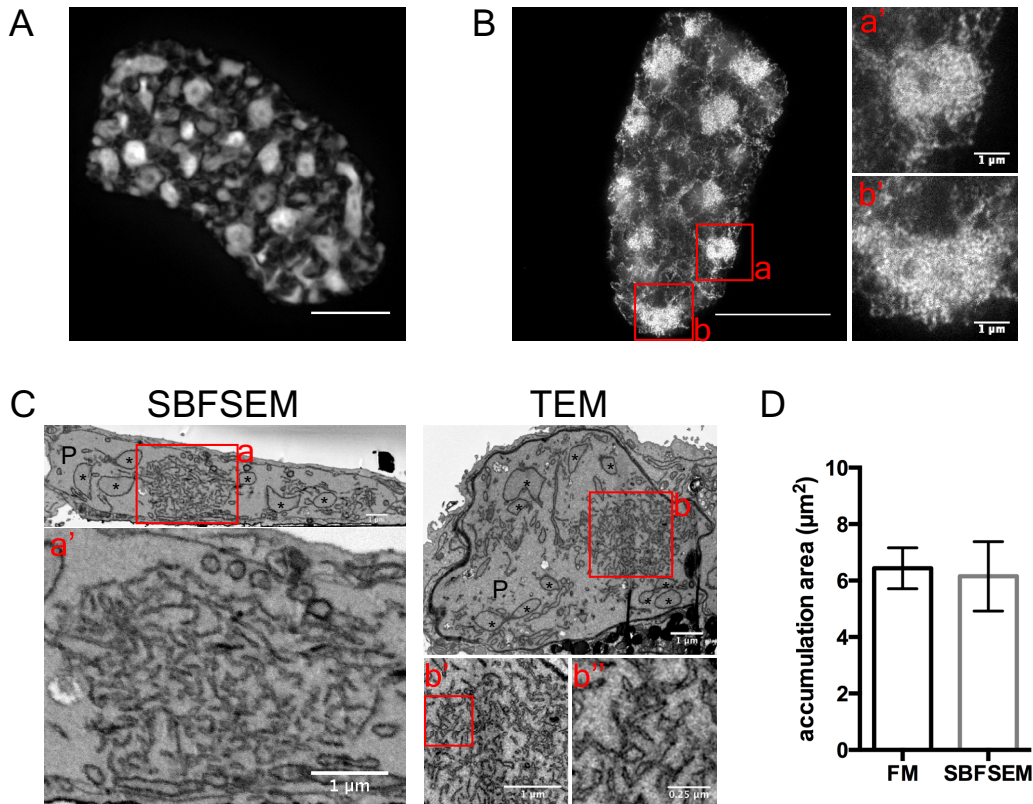A. HeLa cells were infected with WT parasites, fixed at 48 hpi and stained with anti-PbBiP antiserum (green). DNA was visualized with DAPI (blue).
B. HeLa cells were infected with Pb^{C}sfGFP-Sec61β parasites, fixed at 48 hpi and stained with anti-PbBiP antiserum. The sfGFP signal of Pb^{C}sfGFP-Sec61β parasites (green) correlates well to the anti-PbBiP staining (red). The Pearsons's *R* value of both signals in the ROI (red square) was determined and is presented below the right image.
C. Intravital imaging confirms presence of ER accumulations *in vivo*. C57BL/6 mice were infected with Pb^{C}sfGFP-Sec61β parasites and intravital microscopy was performed at either 42 or 49 hpi. ER accumulations are present in schizonts (42 hpi) and absent in parasites that have divided their ER and formed merozoites (49 hpi). Scale bars correspond to 10 μm.

were able to identify parasites containing ER accumulations. SBFSEM imaging confirmed that the ER forms an intricate dense and seemingly interconnected tubular network, which most often has a round to oval shape (Fig. 4C-a and 4C-a′, Supporting Information Fig. S5 and Movie S2 and S3). Using transmission EM (TEM) we were able to obtain an even higher resolution of the tubular network and to resolve ER membranes (Fig. 4C-b, b′, b″). We found that ER tubules within the network have a mean diameter of 68 ± 6 nm (95% confidence interval), which is consistent with the typical ER diameter of 50–100 nm found in most eukaryotic organisms. (Voeltz *et al.*, 2002). We measured the area of ER accumulations at their greatest width in SBFSEM images and compared this with standard FM of parasites, for which infections had been performed identically up to and including parasite fixation. We found that ER accumulations imaged with either SBFSEM or FM have a similar mean area of about 6.3

μm^2 and we, therefore, conclude that structures found by SBFSEM and FM are the same (Fig. 4D).

FLIP analysis of the parasite ER

Having established that the ER consists of vast accumulations in addition to a tubular network and the perinuclear ER, we sought to investigate whether or not these are connected. To get a better understanding of the ER architecture, we performed fluorescence loss in photobleaching (FLIP) experiments in which we repeatedly photobleached a 3.75 μm^2 area of Pb^{C}GFP-Sec61β parasites and measured fluorescence intensity in the remainder of the parasite. If the GFP-tagged protein can diffuse freely throughout the entire parasite ER, we would expect that the fluorescence intensity of the entire ER would rapidly decrease (Teixeira and Huston, 2008). To control for

Fig. 4. High resolution imaging of ER accumulations in *P. berghei* parasites reveals a dense, intricate tubular ER network.
A. HeLa cells were infected with Pb[C]sfGFP-Sec61β parasites and imaged at 48 hpi by live cell imaging using a confocal spinning disc microscope.
B. HeLa cells infected with WT parasites were fixed at 48 hpi, stained with anti-PbBiP antiserum and analysed using STED microscopy. Details a and b are highlighted and displayed additionally at a higher magnification.
C. Ultrastructure of ER accumulations reveals a tubular architecture of ER accumulations. HeLa cells infected with Pb[C]mCherry parasites were fixed at 48 hpi and osmium-stained for EM. Cells were vertically cut and images were taken by SBFSEM (on the left), a′ shows the ER accumulations seen at a higher magnification. Higher resolved images of parasites were acquired using TEM, b′ and b″ show the tubular architecture of ER accumulations in greater detail.
D. ER accumulations of parasites treated identically up to and including fixation, and subsequently imaged with SBFSEM or FM have the same size. Parasites used for FM imaging were stained with anti-PbBiP antiserum. Shown are mean values, the error is depicted as 95% confidence interval. A Mann–Whitney test was performed, showing that the size of accumulations is not different, *P* value = 0.9702, *n* = 2 with more than 20 accumulations measured per setting and replicate. P, parasite; asterisks, parasite nuclei. Scale bars correspond to 10 μm, if not labelled differently.

fluorescence loss by repeated imaging we imaged a separate set of parasites where the bleaching area was set outside the parasite. When we analysed parasites at 40 hpi using FLIP we observed an almost complete loss of fluorescence in the entire parasite ER after 20 cycles of photobleaching. This loss is specific as control parasites show only a minor decrease in fluorescence intensity (Fig. 5A and Supporting Information Movies S4 and S5). These results imply that the GFP-Sec61β fusion protein can diffuse freely throughout what must be a single interconnected ER compartment despite its various forms. We had noticed that the ER seems to be divided shortly before single merozoites are formed and we assumed that the ER has lost its connection through the whole parasite at this point (Fig. 2C). When we photobleached a 3.75 μm^2 area of the parasite ER at 56 hpi, at which point

only perinuclear ER is seen, only minor levels of fluorescence intensity are lost in the remaining parasite, meaning that at this stage, the ER has mostly lost its interconnectivity (Fig. 5B and Supporting Information Movies S6 and S7) confirming our observation made by fluorescence microscopy (Fig. 2C).

Effect of ER stress on ER accumulations in *P. berghei* liver stage parasites

Plasmodium parasites appear to be fairly limited in the machinery they harbour to react to and cope with ER stress (Gosline *et al.*, 2011; Harbut *et al.*, 2012) (Fig. 1). We reasoned that the parasite might, therefore, be much more sensitive to inhibitors that induce ER stress and that inhibitor treatment might have an influence on

A

PbCGFP-Sec61β 40 hpi

B

PbCGFP-Sec61β 56 hpi
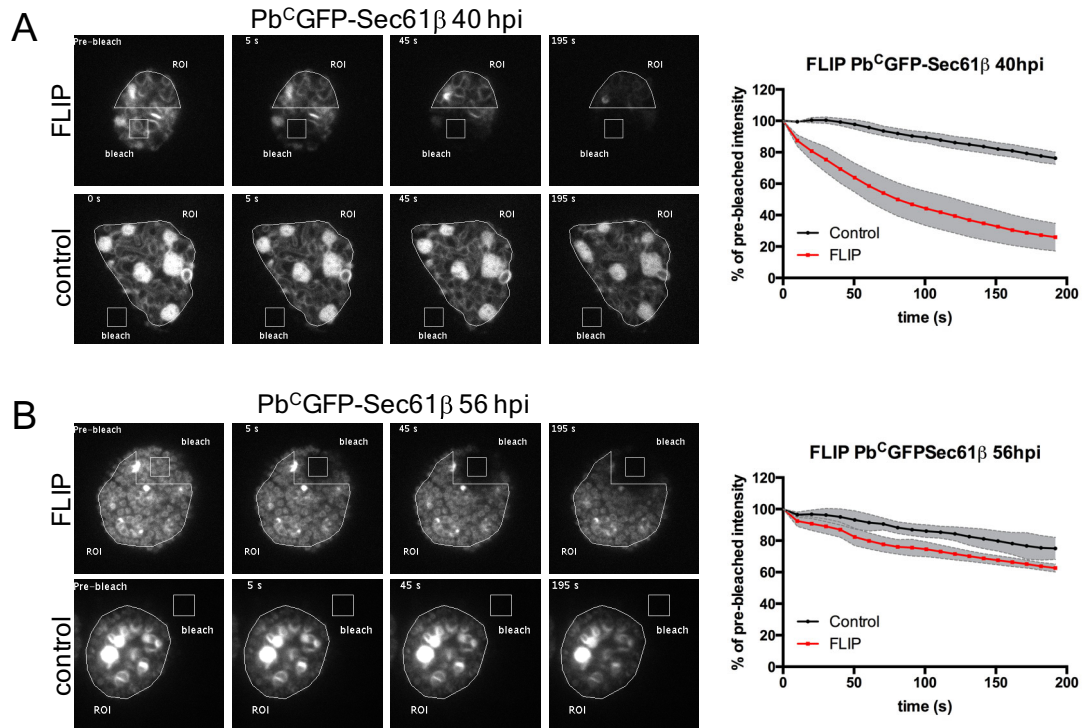
Fig. 5. FLIP imaging of the *P. berghei* ER shows that the parasite ER is a single continuous organelle, which is divided once merozoites are formed. HeLa cells were infected with PbCGFP-Sec61β parasites and imaged live at either 40 hpi A. or 56 hpi B. Parasites were photobleached 20 times at 10 s intervals at the indicated area. Fluorescence intensity was measured at the ROI. In control parasites, the bleaching area was set outside of the parasite to account for loss of fluorescence intensity by imaging. Images of representative parasites are shown. Fluorescence intensity values of the prebleached parasites were set as 100%. Depicted values are means, error is depicted as 95% confidence intervals (grey area above and under the curve) of the relative fluorescence intensity at each time point, $n = 3$, with each eight imaged parasites per settings.

abundance and size of ER accumulations, as ER extension is known to alleviate ER stress (Schuck *et al.*, 2009). Infected cells were treated with inhibitor concentrations that did not affect host cell development, and their effect on parasite development was investigated (Fig. 6 and Supporting Information Fig. S6). ER stress was induced using the well-described proteasome inhibitor MG132 or using two different signal peptide peptidase (SPP) inhibitors, namely (ZLL)$_2$ and Ly411575. MG132 selectively blocks the proteolytic activity of the 26S proteasome, which is known to be present in *Plasmodium* parasites, leading to the accumulation of ubiquitinated proteins and thus ER stress (Aminake *et al.*, 2012; Prasad *et al.*, 2013). (ZLL)$_2$ and Ly411575 have been described to specifically inhibit the activity of *Plasmodium* SPP (Parvanova *et al.*, 2009; Harbut *et al.*, 2012). SPP is an ER-resident protein, which is involved in the removal of signal peptides. In mammalian cells, an additional role has been found in transport of proteins destined for proteasomal degradation from the ER lumen to the cytoplasm (Loureiro *et al.*, 2006). We infected HeLa cells with PbCGFP parasites (PbGFP$_{CON}$, constitutive cytoplasmic GFP expression (Franke-Fayard *et al.*, 2004)) and

initiated inhibitor treatment at 24 hpi (MG132 at 50 nM, (ZLL)$_2$ at 2 μM and Ly411575 at 20 nM). Applied inhibitors did not interfere with host cell growth and proliferation at concentrations used (Supporting Information Fig. S6). At 48 hpi, we visualized the ER with ER-Tracker™ Red, which gives an ER staining that correlates to the previously observed ER localization (Supporting Information Fig. S7A). A confocal spinning disc microscope was used to assess the size and number of ER accumulations in relation to the parasite size of inhibitor-treated parasites compared to control parasites (Fig. 6A). Measured parasites had a comparable thickness along the *z*-dimension (Supporting Information Fig. S7B). Parasites treated with Ly411575 were not assessed for size and number of ER accumulations, since we observed that parasite development was dramatically impaired; parasites stayed very small and did not form any ER accumulations. For untreated parasites and those treated with inhibitors other than Ly411575, we first analysed the mean area of ER accumulations to investigate whether inhibitor treatment influenced the morphology of single ER accumulations independent of the parasite size (Fig. 6B). Next, we investigated if inhibitor-treated parasites harboured
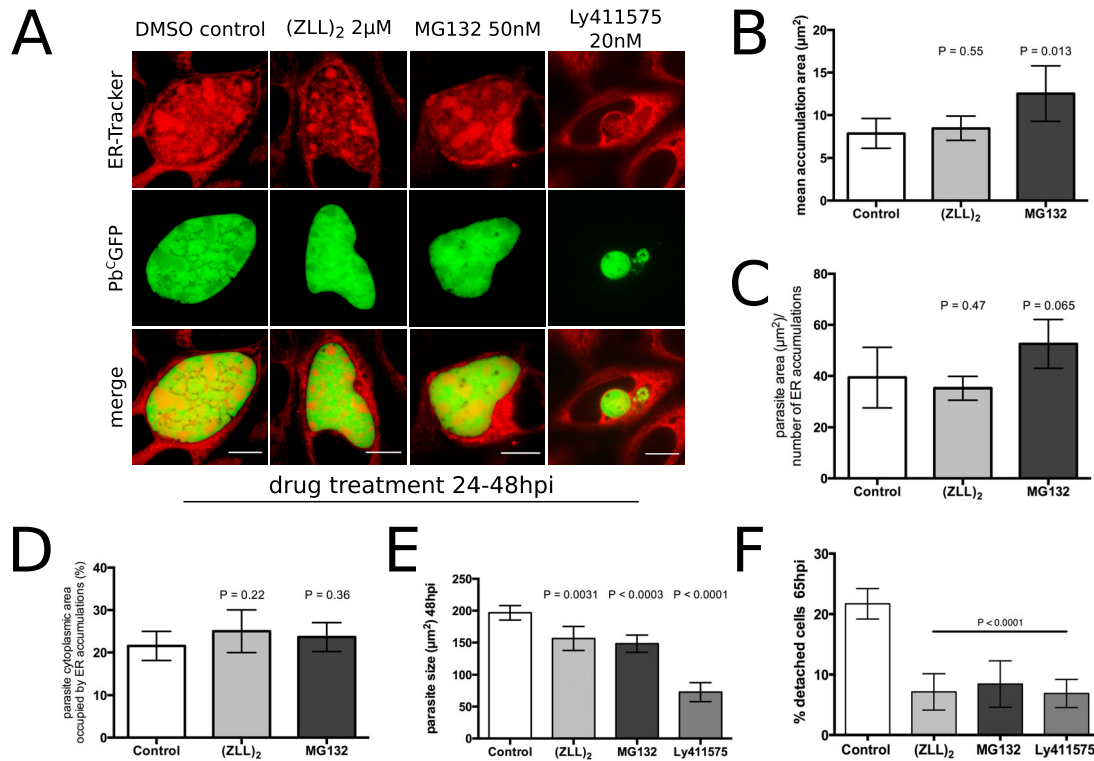
Fig. 6. Treatment of parasites with ER stress-inducing inhibitors MG132, (ZLL)$_2$ and Ly411575 drastically interferes with parasite development. HeLa cells were infected with Pb^{C}GFP (A-D) or Pb^{C}m-Cherry parasites (E, F), either one of the inhibitors (MG132 at 50 nM, (ZLL)$_2$ at 2 μM and Ly411575 at 20 nM) or DMSO for control parasites was added from 24 hpi onwards and exchanged 48 hpi.
A. At 48 hpi, inhibitor-treated Pb^{C}GFP parasites were stained with 500 nM ER-Tracker^{TM} Red and subsequently imaged with a confocal spinning disc microscope. Representative images of the accordingly treated parasites are shown.
B. ER accumulations are bigger in MG132-treated parasites. The area of ER accumulations, at their widest expansion, was measured by density slicing using Fiji, the mean area of ER accumulations of differently treated parasites was calculated.
C. Effect of inhibitor treatment on the number of accumulations in relation to the parasite size. Shown is the parasite area that corresponds to one ER accumulation.
D. Analysis of total expansion of ER accumulations upon inhibitor treatment. The percentage of cytoplasmic parasite area occupied by ER accumulations was calculated. A–D $n = 3$, with 15 parasites measured per treatment and replicate.
E. Inhibitor-treated parasites are significantly smaller than control parasites. Inhibitor-treated and control parasites were imaged live at 48 hpi, parasite size was measured by density slicing using Fiji, $n = 3$, with more than 100 parasites per treatment and replicate.
F. Inhibitor-treated parasites are impaired in successfully completing liver stage development. Inhibitor treated and control parasites were counted at 48 hpi and detached cells were counted in the supernatant at 65 hpi. The ratio of detached cells at 65 hpi to infected HeLa cells at 48 hpi is shown, $n = 3$, with more than 100 parasites per treatment and replicate. Statistical analysis was performed using an unpaired, two-tailed t-test (A–D and F) or a Mann–Whitney test (E). Shown values are means of replicates and the error is depicted as 95% confidence intervals. Scale bars correspond to 10 μm.

different numbers of ER accumulations. As parasites can vary considerably in size, we analysed the total parasite area per ER accumulation (Fig. 6C). Finally, we analysed the total extent of ER accumulations, represented by the percentage of parasite cytoplasmic area occupied by ER accumulations (Fig. 6D). When we treated parasites with MG132, we observed that they form significantly larger ER accumulations, but seem to have slightly (nonsignificantly) reduced numbers of ER accumulations per parasite relative to the parasite area. Nevertheless, the total parasite area that is occupied by ER accumulations seems to be similar in control parasites (Fig. 6B–D). Parasites treated with (ZLL)$_2$ form ER accumulations that are relatively similar in size and number compared to those in control parasites (Fig. 6B–D). In addition to the abundance and size of ER accumulations, we also analysed the effect of inhibitor treatment on parasite size and on completion of liver stage development. Interestingly, we found that parasites treated with ER stress-inducing inhibitors were generally smaller at 48 hpi. This was most significant upon treatment with Ly411575, where parasite size was only half that of control parasites (Fig. 6E). Furthermore, all inhibitor-treated parasites were severely impaired in successfully completing liver stage development, illustrated by a more than 50% reduction in the generation of detached cells compared to control parasites (Fig. 6F).
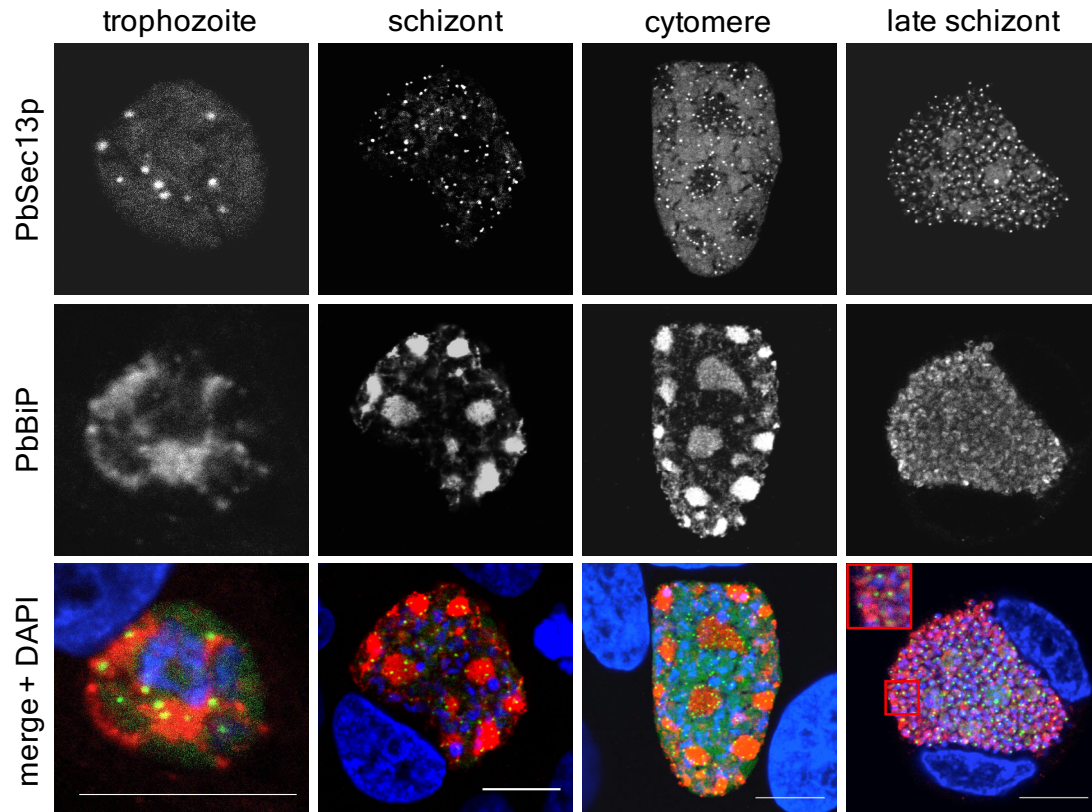
Fig. 7. Translational ER foci, defined by Sec13p-GFP are found at distinct areas of the parasite ER, including at ER accumulations. HeLa cells were infected with Pb^{C}Sec13p-GFP parasites. Cells were fixed at different time points during liver stage development and stained with anti-PbBiP antiserum (red). PbSec13p-GFP (green) is found in distinct regions of the ER membrane. During the cytomere stage, PbSec13p-GFP foci seem to be enriched at ER accumulations. Merozoites each have a single tER site. DNA was stained with DAPI. Scale bars correspond to 10 μm.

Markers of the tER, cis- and trans-Golgi are localized at ER accumulations

To further characterize the role of parasite ER accumulations, we were interested in understanding whether these accumulations are sites of protein synthesis and subsequent transport. For initial characterization of the *P. berghei* ER we used transgenic parasites expressing a (sf)GFP-PbSec61β fusion protein (Fig. 2A–C). Sec61β, together with Sec61α and Sec61γ, builds the Sec61 complex, which forms a channel through the ER membrane and is central to co- and post-translational protein translocation. Membrane-bound ribosomes are known to be tightly associated with the Sec61 complex to facilitate co-translational protein transport (Kelkar and Dobberstein, 2009).

Successfully folded proteins exit the ER at ER subdomains, so-called tER sites, to then be transported to the cis-Golgi for further modification and sorting. Sec13p is a component of COPII-coated vesicles that has been used previously in *P. falciparum* to visualize the tER (Struck *et al.*, 2008b). Here, we generated transgenic parasites expressing the *P. berghei* homologue of Sec13p (PBANKA_144540) as a GFP fusion protein. Pb^{C}Sec13p-GFP-infected HeLa cells were fixed between 24 and 56 hpi and stained with anti-PbBiP antiserum to allow visualization of the ER with tER sites at mid to late liver stage development (Fig. 7). PbSec13p is localized in distinct foci, which we found to be distributed along the parasite ER during the *Plasmodium* liver stage. Interestingly, tER foci are also present at ER accumulations, seemingly concentrated at their periphery. Generally, tER foci appear to be more abundant at ER accumulations than at other sites of the ER. Merozoites of mature schizonts each harbour a single tER site, localized at a distinct region of the parasite perinuclear ER (Fig. 7).

We were next interested in how the Golgi is positioned in relation to the ER. In the cells of most organisms, the cis-Golgi is found juxtaposed to the tER, to allow effective COPII-mediated protein transport between the ER and Golgi apparatus. As *Plasmodium* parasites possess a non-classical unstacked Golgi, the trans-face of the Golgi is found in close proximity to the cis-Golgi. The Golgi reassembling stacking protein (GRASP) and Rab6 are well-established marker proteins of the cis-Golgi and trans-

Golgi, respectively, and have been used in *P. falciparum* for visualization of both Golgi faces in the parasite's blood stage (Struck *et al.*, 2008a,b). To visualize the cis-Golgi and trans-Golgi, we generated Pb^{LS}GRASP-GFP and Pb^{LS}GFP-Rab6 parasites (Supporting Information Figs S8, S9 and S12). Pb^{LS}GRASP-GFP parasites were fixed at different time points of liver stage development and the ER was stained with anti-PbBiP antiserum. Cis-Golgi faces are found at distinct ER sites, with the cis-Golgi being mostly found at ER accumulations (Supporting Information Fig. S8). To verify these observations, we additionally generated double fluorescent Pb^{C}sfGFP-Sec61β-Pb^{LS}GRASP-mCherry parasites. Confocal live cell imaging of these double-fluorescent parasites confirmed that cis-Golgi faces are indeed mainly found at ER accumulations (Fig. 8 and Supporting Information Movies S8 and S9). Interestingly, when the PM starts to invaginate at the cytomere stage, cis-Golgi structures are found underlying the PM and become absent from ER accumulations. Following this, each forming daughter merozoite was observed to inherit one cis-Golgi face, which is then localized at a distinct site of the perinuclear ER (Fig. 8). For analysis of the trans-Golgi localization, Pb^{LS}GFP-Rab6 parasites were stained with ER-Tracker^{TM} Red and imaged live. Interestingly, we found that trans-Golgi faces are also localized at ER accumulations but are also frequently located at other regions of the ER (Supporting Information Fig. S9). Finally, when single merozoites are formed, they contain a single cis- and trans-Golgi face (Supporting Information Figs S8 and S9). In summary, we find that tER and cis- and trans-Golgi compartments are localized at ER accumulations and hence we suggest that ER accumulations might be hubs of protein export from the ER to the Golgi apparatus.

The ER forms extensions towards the parasite plasma membrane and parasitophorous vacuole membrane

Visualizing the parasite ER by confocal imaging of sfGFP-tagged Sec61β and ER-Tracker^{TM} Red and by EM, we noticed that the ER not only forms a huge network throughout the parasite but also seemingly extends towards the parasite PM and even to the PVM (Fig. 9A). To further investigate this observation, HeLa cells were infected with Pb^{LS}Exp1-GFP parasites, which express the PVM-resident protein PbExp1 (*P. berghei* exported protein 1), fused to GFP. Pb^{LS}Exp1-GFP parasites were found to develop similarly to Pb^{LS}Exp1-mCherry parasites (Graewe *et al.*, 2011). At 48 hpi parasites were stained with ER-Tracker^{TM} Red and imaged using a confocal spinning disc microscope. We observed that the parasite ER forms long tubular extensions towards the PVM, often originating from node-like ER structures close to the PM (Fig. 9A, red arrows). Tubular extensions are different ER structures

than the previously described ER accumulations. Interestingly, we found that the PVM is also stained by ER-Tracker^{TM}, which is a drug conjugate glibenclamide BODIPY® TR (Fig. 9A). Glibenclamides are known to bind selectively to sulphonylurea receptors of ATP-sensitive K$^+$ channels, prominent on the ER (Hambrock *et al.*, 2002). Due to the staining of the PVM with ER-Tracker^{TM}, we hypothesized that the ER potentially feeds lipids into the PVM. Interestingly, we found that staining of the PVM by ER-Tracker^{TM} is most obvious in regions where the PbExp1-GFP signal is weak or absent (Fig. 9A, white arrows). Seeking to characterize the spatiotemporal presence of ER extensions directed towards the parasite periphery we imaged Pb^{LS}Exp1-GFP, PbWT and Pb^{C}GFP parasites stained with ER-Tracker^{TM} Red, live at different time points throughout liver stage development. We found ER extensions in all imaged parasites at each time point investigated between 24 hpi and 56 hpi ($n > 3$, with more than 15 parasites imaged per replicate and time point). Data of Pb^{LS}Exp1-GFP and PbWT are not shown, examples of imaged Pb^{C}GFP parasites are provided in Supporting Information Fig. S10A. Live imaging of transgenic double fluorescent Pb^{C}sfGFP-Sec61β-Pb^{LS}Exp1-mCherry parasites allowed detailed analysis of parasite ER and PVM dynamics without potential artefacts through live stains or fixation. We imaged parasites during liver stage development (40, 48 and 56 hpi) using a confocal microscope and were able to confirm the presence of ER extensions towards the PVM in all imaged parasites ($n = 3$ per time point, with each 20 imaged parasites per replicate) (Fig. 9B upper panel, arrows and Supporting Information Fig. S10B). Pb^{C}sfGFP-Sec61β-Pb^{LS}Exp1-mCherry parasites, fixed at 48 hpi were imaged at a higher resolution using STED microscopy, which indicates that tubules of the parasite ER seemingly interlace with the PVM and/or PM to establish potential ER-PM/PVM contact sites (Fig. 9B lower panel, arrows). In addition to our observations made using confocal microscopy, we also detected potential connections between the ER and the parasite PM and/or PVM by SBFSEM, which again seem to originate from a node-like ER structure close to the PM. Thus, EM data strengthens our observation of potential contact sites between the ER and the parasite PM and/or PVM (Fig. 9C).

Discussion

Here, we report for the first time a detailed description of highly concentrated ER accumulations that are evenly distributed within and formed during development of *Plasmodium* parasites, additionally to an interconnected perinuclear and network-like parasite ER. A combination of high-resolution STED microscopy and SBFSEM allowed us to define ER
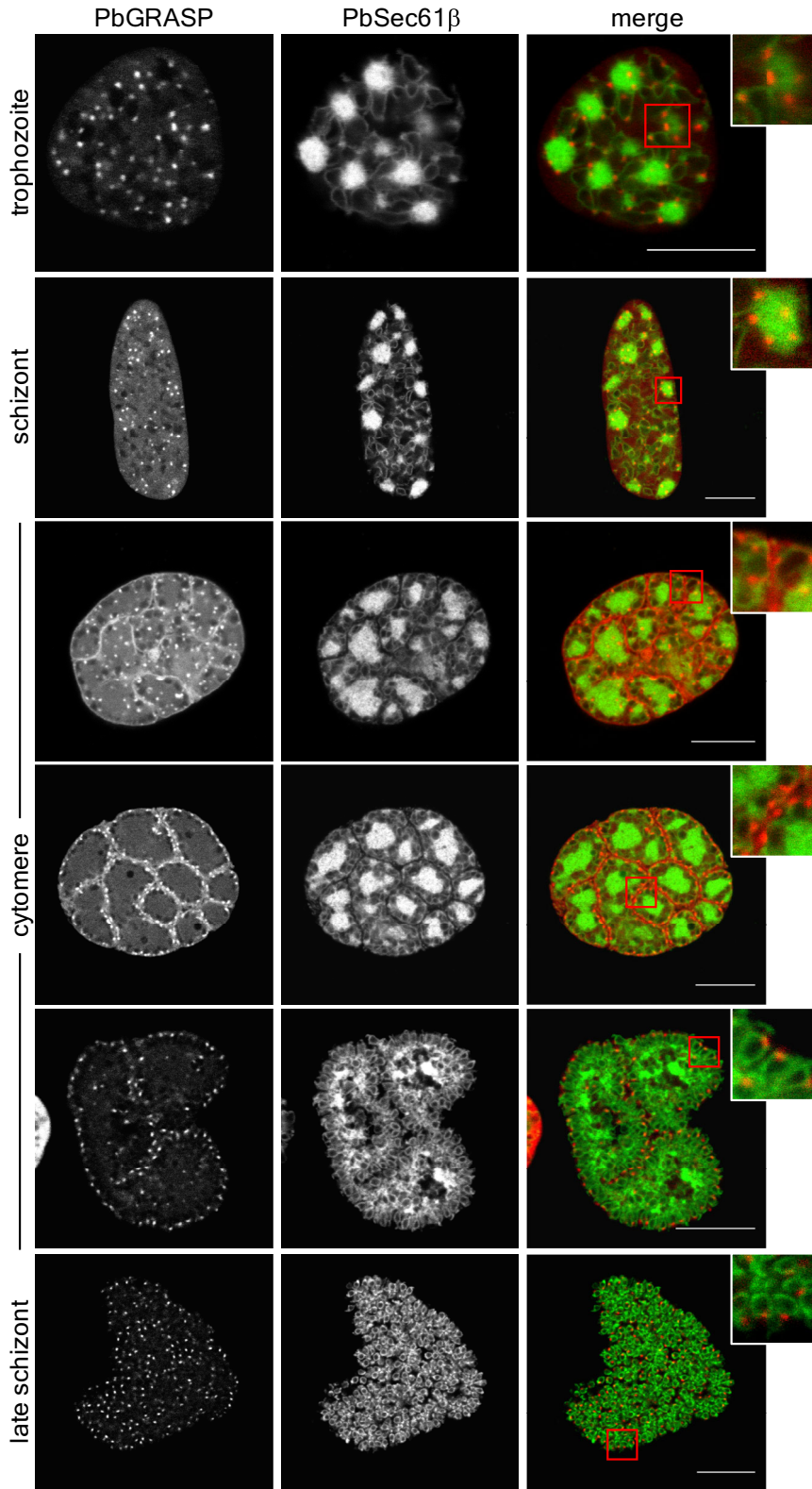
Fig. 8. The cis-Golgi (red), defined by PbGRASP-mCherry, is localized at distinct regions of the parasite ER (green). HeLa cells were infected with Pb^{C}sfGFP-Sec61β-Pb^{LS}GRASP-mCherry. Cells were imaged live with a confocal microscope at different time points of parasite liver stage development between 36 and 56 hpi. Between the trophozoite and cytomere stage, cis-Golgi structures are mainly present at ER accumulations. Upon parasite PM invagination around groups of nuclei the cis-Golgi is found at the parasite periphery and absent from ER accumulations. Merozoites each contain one cis-Golgi face. Red boxes are shown at a higher magnification. Scale bars correspond to 10 μm.
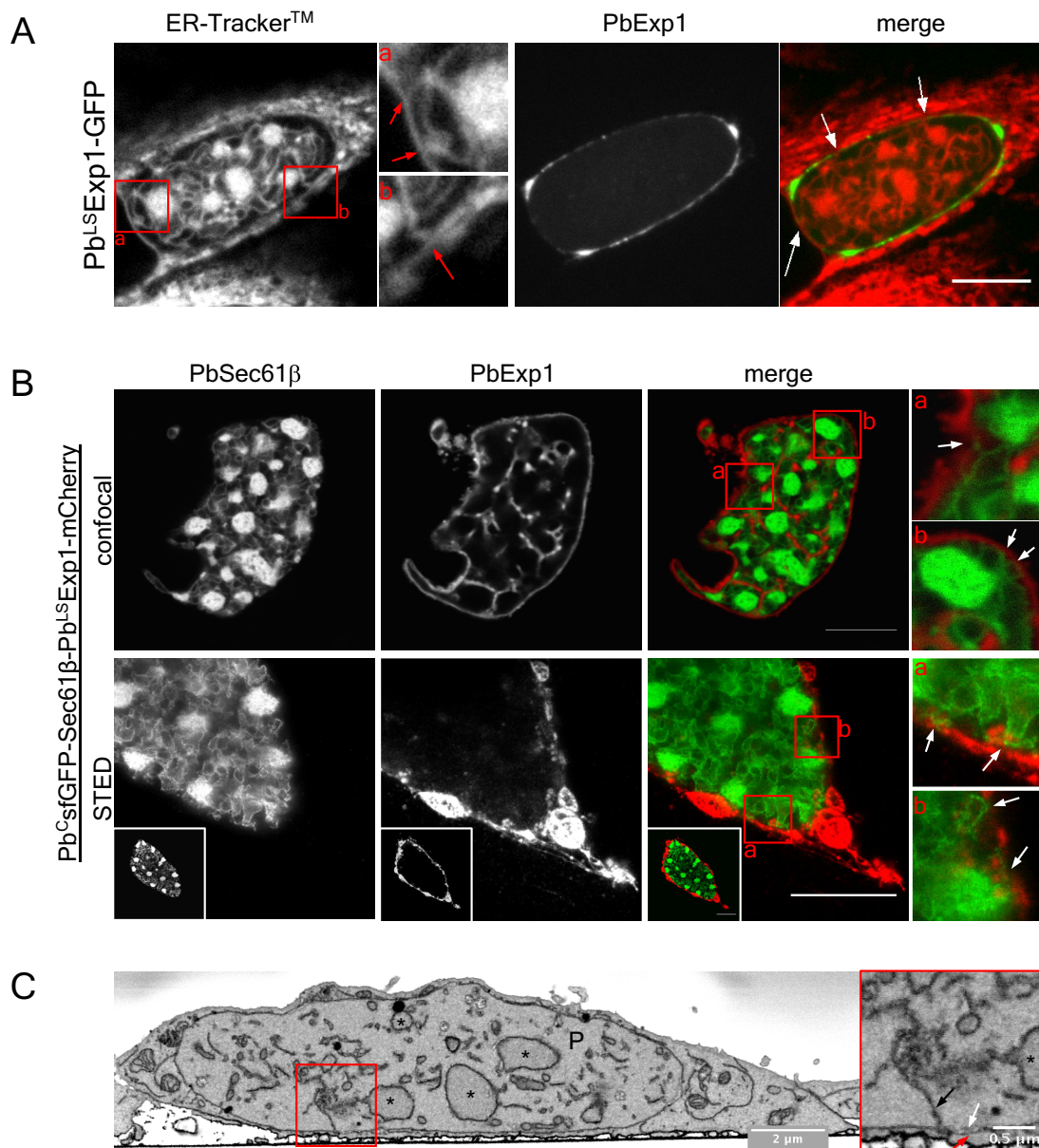
Fig. 9. The parasite ER forms extensions towards the parasite PVM and/or underlying PM. HeLa cells were infected with Pb^LS^Exp1-GFP (A), Pb^C^sfGFP-Sec61β-Pb^LS^Exp1-mCherry (B) or Pb^C^mCherry (C) parasites. A. At 48 hpi Pb^LS^Exp1-GFP parasites were stained with 500 nM ER-Tracker^TM^ Red and imaged with a confocal spinning disc microscope. Boxed areas a and b are shown with a higher magnification on the right side, depicting the ER extensions towards the PVM. Red arrows indicate potential contact sites of the parasite ER with the PM and or PVM. White arrows show areas of the PVM where the staining with ER-Tracker^TM^ Red is more dominant than the GFP signal of Pb^LS^Exp1-GFP parasites, which seems to be weaker at these regions. B. At 48 hpi Pb^C^sfGFP-Sec61β-Pb^LS^Exp1-mCherry parasites were imaged live with a confocal microscope (upper panel) or fixed using STED microscopy (lower panel). Boxed areas a and b are shown at a higher magnification and arrows indicate ER extensions towards the PVM. C. Pb^C^mCherry parasites were fixed at 48 hpi and osmium-stained for EM. Images were acquired using SBFSEM. The boxed area is shown at a higher magnification on the right side and shows a node-like ER structure with an extension (black arrow) towards the parasite PM and or PVM (white arrow). P, parasite; asterisks, parasite nuclei. Scale bars correspond to 10 μm, if not labelled differently.

accumulations as an intricate network of densely packed ER tubules.

Even though the *Plasmodium* ER has been the focus of numerous studies, ER accumulations as described in the present study, have never been mentioned. Couffin et al. showed that *P. falciparum* Sec61 is localized at the parasite ER in blood stage parasites using antibody staining. Although FM images cannot be interpreted conclusively and blood stage parasites are much smaller than liver stage parasites, one can already identify ER accumulations in their staining (Couffin *et al.*, 1998). Another study characterized ER morphology in *P. falciparum* blood stage parasites expressing GFP with an ER retention signal -SDEL. They describe the parasite ER,

similarly to our observations, as a ring around the nucleus that forms extensions into the cytoplasm, which become considerably branched in late stages. However, ER accumulations, clearly present in their images of transgenic trophozoites and schizont parasites are not mentioned in the text (van Dooren *et al.*, 2005). Similarly, other studies investigating vesicle-mediated trafficking, PfSec22, PfSec24 and PfSec12 of the *P. falciparum* blood stage also show images of the parasite ER with visible ER accumulations, but these were not made reference to (Adisa *et al.*, 2007; Lee *et al.*, 2008; Ayong *et al.*, 2009). Additionally, a recent study using *P. yoelii* liver stage parasites found the lysophosphatidic acid acyltransferase (LPAAT) PY01678 to be localized at the parasite ER. Staining of the *P. yoelii* ER with anti-BiP in this study clearly shows the presence of numerous ER accumulations in *P. yoelii* liver stage parasites, which were again not discussed (Lindner *et al.*, 2014).

The ER size and shape is highly dependent on the function and requirements of the cell. For example, the ER of B lymphocytes triples its size during differentiation into highly secreting plasma cells, which are clearly in need of a greater protein folding capacity (Van Anken *et al.*, 2003). The UPR has been shown to play an essential role in the expansion of ER membranes. Under ER stress, the transcription factor XBP1 is activated by IRE1, leading to the elevation of the chaperone level in the ER. Additionally, UPR activates the associated ERAD and lipid biosynthesis pathway (Cox *et al.*, 1997). Accordingly, XBP1-deficient B lymphocytes are not able to differentiate into plasma cells as they fail to expand their ER (Reimold *et al.*, 2001). Interestingly, yeast cells deficient in either IRE1 or Hac1 (XBP1 in metazoans) were not able to normally expand their ER membrane by generation of ER sheets but instead expanded their ER through formation of ER patches under ER stress (Schuck *et al.*, 2009). Using EM, they were identified as abnormally shaped, intertwined ER tubules. Surprisingly, even though ER expansion in UPR-deficient yeast cells was based on tubular expansion and was uncoupled from increasing amounts of chaperones, ER expansion alone, independent of its shape, was sufficient to alleviate ER stress (Schuck *et al.*, 2009). ER patches identified in yeast are quite similar in their organization to ER accumulations we observed during *Plasmodium* asexual development. Bearing in mind that *Plasmodium* parasites harbour only a dramatically reduced UPR machinery, deficient in IRE1, AFT6 and their downstream components and are thus limited in their response to ER stress (Fig. 1), ER accumulations might indeed be generated to alleviate the ER stress caused by the enormous growth rate of the parasite (Gosline *et al.*, 2011). Upon inhibitor treatment, we observed only a tendency for the total parasite

area occupied by ER accumulations to be slightly larger in inhibitor-treated parasites than in control parasites. A possible reason we do not see more significant effects on the size and number of ER accumulations, when ER stress is induced with inhibitors, is that parasites might already have an intrinsically increased level of ER stress, defined by ER expansion, as a result of the tremendous parasite growth rate. As a consequence, inhibitor-induced ER stress might shift the ER stress response from seeking to restore ER homeostasis towards a cell death response. This hypothesis is supported by the fact that we observed a clear reduction in the number of successfully developing parasites and in parasite size, upon treatment with ER stress-inducing inhibitors. The fact that *Plasmodium* parasites harbour a vastly reduced UPR machinery and the elevated sensitivity of parasites to ER stress, illustrate the potential of interfering with parasite development by targeting components of the parasite UPR.

Using classical marker proteins of the tER, cis- and trans-Golgi, we have examined the relationship between ER accumulations and the immediate secretory system. We found that foci of ER exit sites and Golgi cisternae are concentrated at ER accumulations. Accordingly, we assume that ER accumulations are functional divisions of the parasite ER, involved in protein and lipid dispatch.

Once parasites have finished nuclear division and start to build merozoites, we noticed by *in vitro* and intravital live cell imaging that ER accumulations disappear. It is believed that the parasite PM needed to encase forming merozoites originates from invaginations of the surrounding PM, primarily around spheres of nuclei, and finally around single merozoites. Invagination of the PM to form single merozoites is restricted to a short period of time spanning only a few hours at the end of parasite development (Sturm *et al.*, 2009; Stanway *et al.*, 2011). Little is known about how the parasite is able to provide sufficient amounts of membrane to surround thousands of merozoites in such a short time frame. In *Plasmodium* parasites, membrane reservoirs are not found directly at the PM but rather at the surrounding PVM, which forms extensive protrusions into the parasite host cell during liver and blood stage development (Deschermeier *et al.*, 2012; Grützke *et al.*, 2014; Prado *et al.*, 2015; Matz *et al.*, 2015). The PM and PVM exhibit regions of close alignment, which would theoretically allow for a direct exchange of membranous material between the two membranes. However, as the parasite matures and especially when the PM starts to invaginate, the distance between PM and PVM increases (Graewe *et al.*, 2011), hindering potential membrane transfer. We have observed by live cell imaging and EM that the parasite ER extends tubules from node-like ER patches towards the parasite PVM

and/or PM, appearing to build up membrane contact sites. Based on these findings, we hypothesize that lipids might be transferred directly via ER-PM contact sites to allow for PM expansion and invagination. In other eukaryotes, ER-PM contact sites are involved in many cellular processes, such as nonvesicular lipid transport, store-operated Ca^{2+} entry and cell signalling (Henne *et al.*, 2015). Since we could never observe direct transport of proteins, such as sfGFP-PbSec61β, through ER-PM contact sites, we propose that membrane lipids might be transported via non-vesicular lipid transport from the ER to the PM rather than through membrane fusion or vesicular transport.

Here, we provide first observations of potential contact sites between the parasite ER and PM, yet further investigations are needed to analyse whether lipids are transferred via MCSs and if potential transfer leads to the depletion of ER accumulations and helps membrane expansion.

In summary, the use of high-end microscopy techniques has enabled us to analyse the morphology of the *P. berghei* ER in detail and to provide explanations regarding the origin and function of ER accumulations identified.

Experimental procedures

Animal work statement

Experiments were conducted with strict accordance to the guidelines of the Swiss Tierschutzgesetz (TSchG; Animal Rights Laws) and approved by the ethical committee of the University of Bern (Permit Number: BE109/13).

C57BL/6 and BALB/c mice used in experiments were between 6 and 10 weeks of age and were either bred in the central animal facility of the University of Bern, or were supplied from Harlan Laboratories or Charles River.

Culture and *in vitro* infection of HeLa cells

In this study, we used HeLa cells, which in contrast to HepG2 cells, grow only in a single layer. On the one hand, this allows sporozoites to infect host cells more easily, which results in a higher infection rate and on the other hand facilitates imaging of subcellular structures of *P. berghei* liver stages *in vitro*. Development of parasites in HeLa cells and HepG2 cells to infectious merozoites is comparable. It has been previously demonstrated that *P. berghei* parasites are able to successfully develop in HeLa cells (Calvo-Calle *et al.*, 1994). HeLa cells (generous gift from Robert Menard, Pasteur Institute, Paris) were grown in MEM (minimum essential medium) with Earle's salts, supplemented with 10% heat inactivated FCS (foetal calf serum), 1% penicillin/streptomycin and 1% ʟ-glutamine (PAA Laboratories) in a humid incubator at 37°C with 5% CO_2. Cells were passaged twice a week using accutase. For infection, either 3×10^4 cells were seeded onto glass cover slips contained separately in wells of a 24-well cell culture plate, or 1×10^5 cells seeded into glass-bottom dishes. About 24 h post

seeding, HeLa cells were infected with sporozoites prepared from salivary glands of female *Anopheles stephensi* mosquitoes infected with the aforementioned *P. berghei* parasite lines. Sporozoites contained in infection medium [MEM with 2.5 μg ml^{-1} Amphotericin B (PAA Laboratories)] were incubated with HeLa cells for 2 h and following this, the sporozoite-containing medium was removed and new infection medium was added. Afterwards medium was changed daily.

Inhibitor treatment and ER-Tracker™ staining

Inhibitors were dissolved in DMSO for working stocks (MG-132 (Sigma-Aldrich) at 250 μM, (ZLL)$_2$ (Calbiochem) at 10 mM and Ly411575 (Sigma-Aldrich) at 100 μM). HeLa cells were infected with sporozoites of Pb^{C}GFP parasites, inhibitors (MG132 at 50 nM, (ZLL)$_2$ at 2 μM and Ly411575 at 20 nM) were added initially at 24 hpi and exchanged at 48 hpi. For microscopic evaluation of ER accumulations at 48 hpi, the ER was stained using ER-Tracker™ Red (glibenclamide BODIPY® TR). Infected HeLa cells were incubated with 500 nM ER-Tracker™ Red for 1 h at 37°C and 5% CO_2. As a next step, the staining solution was replaced with probe-free infection medium and parasites were imaged no later than 45 min after staining.

Detached cell assay and size measurement

For quantification of parasites that are able to successfully complete liver stage development, HeLa cells were infected as described above. Parasite numbers were counted at 48 hpi and compared to the number of successfully developed parasites (detached cells) that were counted in the supernatant at 65 hpi. The parasite area in μm^2 was measured at 48 hpi by density slicing using Fiji software. Counting and imaging for the size measurement was performed using a Leica DMI6000B widefield epifluorescence microscope.

Live cell imaging and FLIP analysis

For live cell imaging, 1×10^5 HeLa cells were seeded into glass bottom dishes (MatTek) and infected as described, DNA was stained with a final concentration of 1 μg ml^{-1} Hoechst 33342 (Sigma) and cells were kept in 5% CO2 at 37°C. Imaging and time-lapse microscopy were performed using the Leica DMI6000B widefield epifluorescence microscope (Wetzlar) with a Leica HCX PL APO 100× 1.4 oil objective and the Leica LAS AF software. Confocal live cell images of parasites were acquired using the Leica TCS SP8 confocal microscope with the HC PL APO 63×/1.40 oil objective and the Leica Application Suite X software. Imaging of Pb^{C}GFP parasites stained with ER-Tracker™ Red and FLIP analysis of Pb^{C}GFP-Sec61β parasites was performed using a confocal spinning disc microscope (Till Photonics) and a 60× oil objective (numerical aperture 1.35). For FLIP analysis, a bleaching area of 3.75 μm^2 was selected within the parasite and for the control analysis, to account for bleaching by imaging, outside of the parasite. Fluorescence intensity (ROI) was measured for the whole parasite apart from the bleaching area plus a 1.5 μm wide

threshold region. A region outside of the cell was selected for background correction. After acquiring three pre-bleach images, bleaching was performed using 100% power of a 488 nm solid-state laser with five iterations per bleaching. Parasites were bleached 20 times at 10 s intervals and fluorescence intensity was normalized to the mean intensity of the corresponding prebleached images.

In vivo *analysis of PbSec61β parasites*

Pb[C]sfGFP-Sec61β (250,000) sporozoites were injected intravenously into C57BL/6 mice. Intravital microscopy was performed as previously published (Thiberge *et al.*, 2007) at either 42 or 49 hpi using the LSM 510 Zeiss microscope in the LSM 5 live mode. Images were acquired by confocal line scanning microscopy with the Zeiss Plan-Apochromat 63×/1.40 oil DIC M27 objective and the Zeiss LSM 5 Duo Release software.

Serial block-face scanning electron microscopy and transmission electron microscopy

HeLa cells (5×10^4) were seeded per well into a 96-well plate and infected with Pb[C]mCherry parasites, as described above. Infected cells were FACS-sorted at 6 hpi for Pb[C]mCherry infected cells and re-seeded at a density of 10,000 sorted cells per well into a 96-well optical plate (Greiner bio one). Following this, parasites were fixed in a glutaraldehyde buffer at 48 hpi and processed according to a previously published protocol (Deerinck *et al.*, 2010). SBFSEM images were acquired with a Quanta FEG 250 (FEI Company) equipped with a Gatan 3View2XP ultramicrotome (accelerating voltage = 3.5 kV; low vacuum). TEM images were acquired using a Philips/FEI CM12 Transmission Electron Microscope. Images were processed using Fiji.

Statistical analysis

Statistical analysis was conducted with GraphPad Prism version 6.0. An unpaired, two-tailed *t*-test was used for analysing data of the detached cell assay and for analysing the nature of ER accumulations of inhibitor-treated parasites. The Mann–Whitney test was used to analyse the size of parasites treated with inhibitors and to compare accumulation sizes measured either with the Leica DMI6000B widefield epifluorescence microscope or SBFSEM. Experiments were conducted in biological triplicates. The error is depicted as 95% confidence intervals. *P* values < 0.05 were considered significant.

Author contributions

Conception or design of the study: GK, RRS, VTH. Acquisition, analysis or interpretation of the data: GK, RRS, BZ, BK, MDN, PCB, VTH. Writing of the manuscript: GK, VTH, RRS. All authors read and approved the final manuscript.

References

Adisa, A., Frankland, S., Rug, M., Jackson, K., Maier, A.G., Walsh, P., *et al.* (2007) Re-assessing the locations of components of the classical vesicle-mediated trafficking machinery in transfected *Plasmodium falciparum*. *Int J Parasitol* **37**: 1127–1141.

Aminake, M.N., Arndt, H.D., and Pradel, G. (2012) The proteasome of malaria parasites: a multi-stage drug target for chemotherapeutic intervention?. *Int J Parasitol Drugs Drug Resist* **2**: 1–10.

Anken, E.V., Romijn, E.P., Maggioni, C., Mezghrani, A., Sitia, R., Braakman, I., and Heck, A.J.R. (2003) Sequential waves of functionally related proteins are expressed when B cells prepare for antibody secretion. *Immunity* **18**: 243–253.

Ayong, L., Raghavan, A., Schneider, T.G., Taraschi, T.F., Fidock, D.A., and Chakrabarti, D. (2009) The longin domain regulates the steady-state dynamics of Sec22 in Plasmodium falciparum. *Eukaryot Cell* **8**: 1330–1340.

Bano, N., Romano, J.D., Jayabalasingham, B., and Coppens, I. (2007) Cellular interactions of Plasmodium liver stage with its host mammalian cell. *Int J Parasitol* **37**: 1329–1341.

Blume, M., Hliscs, M., Rodriguez-Contreras, D., Sanchez, M., Landfear, S., Lucius, R., *et al.* (2011) A constitutive pan-hexose permease for the Plasmodium life cycle and transgenic models for screening of antimalarial sugar analogs. *FASEB J* **25**: 1218–1229.

Burda, P.C., Roelli, M.A., Schaffner, M., Khan, S.M., Janse, C.J., and Heussler, V.T. (2015) A plasmodium phospholipase is involved in disruption of the liver stage parasitophorous vacuole membrane. *PLOS Pathog* **11**: e1004760.

Calvo-Calle, J., Moreno, A., Eling, W., and Nardin, E. (1994) In vitro development of infectious liver stages of *P. yoelii* and *P. berghei* malaria in human cell lines. *Exp Parasitol* **79**: 362–373.

Costantini, L., and Snapp, E. (2013) Probing endoplasmic reticulum dynamics using fluorescence imaging and photobleaching techniques. In *Current Protocols in Cell Biology*. Hoboken, NJ: Wiley, pp. 21.7.1–21.7.29.

Couffin, S., Hernandez-Rivas, R., Blisnick, T., and Mattei, D. (1998) Characterisation of PfSec61, a Plasmodium falciparum homologue of a component of the translocation machinery at the endoplasmic reticulum membrane of eukaryotic cells. *Mol Biochem Parasitol* **92**: 89–98.

Cox, J.S., Chapman, R.E., and Walter, P. (1997) The unfolded protein response coordinates the production of endoplasmic reticulum protein and endoplasmic reticulum membrane. *Mol Biol Cell* **8**: 1805–1814.

Deerinck, T.J., Bushong, E.A., Thor, A., and Ellisman, M.H. (2010) NCMIR methods for 3D EM: a new protocol for preparation of biological specimens for serial block face scanning electron microscopy. *Microscopy* 6–8.

Deschermeier, C., Hecht, L.S.S., Bach, F., Rützel, K., Stanway, R.R., Nagel, A., *et al.* (2012) Mitochondrial lipoic acid scavenging is essential for *Plasmodium berghei* liver stage development. *Cell Microbiol* **14**: 416–430.

Dooren, G.G.V., Marti, M., Tonkin, C.J., Stimmler, L.M., Cowman, A.F., and McFadden, G.I. (2005) Development of the endoplasmic reticulum, mitochondrion and apicoplast during the asexual life cycle of Plasmodium falciparum. *Mol Microbiol* **57**: 405–419.

Franke-Fayard, B., Trueman, H., Ramesar, J., Mendoza, J., van der Keur, M., van der Linden, R., *et al.* (2004) A *Plasmodium berghei* reference line that constitutively expresses GFP at a high level throughout the complete life cycle. *Mol Biochem Parasitol* **137**: 23–33.

Frischknecht, F., Baldacci, P., Martin, B., Zimmer, C., Thiberge, S., Olivo-Marin, J.C., *et al.* (2004) Imaging movement of malaria parasites during transmission by Anopheles mosquitoes. *Cell Microbiol* **6**: 687–694.

Gosline, S.J.C., Nascimento, M., McCall, L.I., Zilberstein, D., Thomas, D.Y., Matlashewski, G., and Hallett, M. (2011) Intracellular eukaryotic parasites have a distinct unfolded protein response. *PLoS One* **6**: e19118.

Graewe, S., Rankin, K.E., Lehmann, C., Deschermeier, C., Hecht, L., Froehlke, U., *et al.* (2011) Hostile takeover by Plasmodium: reorganization of parasite and host cell membranes during liver stage egress. *PLoS Pathog* **7**: e1002224.

Grützke, J., Rindte, K., Goosmann, C., Silvie, O., Rauch, C., Heuer, D., *et al.* (2014) The spatiotemporal dynamics and membranous features of the Plasmodium liver stage tubovesicular network. *Traffic* **15**: 362–382.

Hambrock, A., Loffler-Walz, C., and Quast, U. (2002) Glibenclamide binding to sulphonylurea receptor subtypes: dependence on adenine nucleotides. *Br J Pharmacol* **136**: 995–1004.

Hammond, A.T., and Glick, B.S. (2000) Dynamics of transitional endoplasmic reticulum sites in vertebrate cells. *Mol Biol Cell* **11**: 3013–3030.

Hanssen, E., Dekiwadia, C., Riglar, D.T., Rug, M., Lemgruber, L., Cowman, A.F., *et al.* (2013) Electron tomography of *Plasmodium falciparum* merozoites reveals core cellular events that underpin erythrocyte invasion. *Cell Microbiol* **15**: 1457–1472.

Harbut, M.B., Patel, B.A., Yeung, B.K.S., McNamara, C.W., Bright, A.T., Ballard, J., *et al.* (2012) Targeting the ERAD pathway via inhibition of signal peptide peptidase for antiparasitic therapeutic design. *Proc Natl Acad Sci USA* **109**: 21486–21491.

Hell, S.W., and Wichman, J. (1994) Breaking the diffraction resolution limit by stimulated emission: stimulated-emission-depletion fluorescence microscopy. *Opt Lett* **19**: 780–782.

Helm, S., Lehmann, C., Nagel, A., Stanway, R.R., Horstmann, S., Llinas, M., and Heussler, V.T. (2010) Identification and characterization of a liver stage-specific promoter region of the malaria parasite Plasmodium. *PLoS One* **5**: e13653.

Henne, W.M., Liou, J., and Emr, S.D. (2015) Molecular mechanisms of inter-organelle ER-PM contact sites. *Curr Opin Cell Biol* **35**: 123–130.

Itoe, M.A., Sampaio, J.L., and Mota, M.M. (2014) Host cell phosphatidylcholine is a key mediator of malaria parasite survival during liver stage infection. *Cell Host Microbe* **16**: 778–786.

Janse, C.J., Franke-Fayard, B., Mair, G.R., Ramesar, J., Thiel, C., Engelmann, S., *et al.* (2006) High efficiency transfection of *Plasmodium berghei* facilitates novel selection procedures. *Mol Biochem Parasitol* **145**: 60–70.

Janssens, S., Pulendran, B., and Lambrecht, B.N. (2014) Emerging functions of the unfolded protein response in immunity. *Nat Immunol* **15**: 910–919.

Joyce, B.R., Tampaki, Z., Kim, K., Wek, R.C., and Sullivan, W.J. (2013) The unfolded protein response in the protozoan parasite *Toxoplasma gondii* features translational and transcriptional control. *Eukaryot Cell* **12**: 979–989.

Kelkar, A., and Dobberstein, B. (2009) Sec61beta, a subunit of the Sec61 protein translocation channel at the endoplasmic reticulum, is involved in the transport of Gurken to the plasma membrane. *BMC Cell Biol* **10**: 11.

Kornmann, B., and Walter, P. (2010) ERMES-mediated ER-mitochondria contacts: molecular hubs for the regulation of mitochondrial biology. *J Cell Sci* **123**: 1389–1393.

Kornmann, B., Osman, C., and Walter, P. (2011) The conserved GTPase Gem1 regulates endoplasmic reticulum-mitochondria connections. *Proc Natl Acad Sci USA* **108**: 14151–14156.

Kumar, N., Koski, G., Harada, M., Aikawa, M., and Zheng, H. (1991) Induction and localization of *Plasmodium falciparum* stress proteins related to the heat shock protein 70 family. *Mol Biochem Parasitol* **48**: 47–58.

Lee, M.C.S., Moura, P.A., Miller, E.A., and Fidock, D.A. (2008) *Plasmodium falciparum* Sec24 marks transitional ER that exports a model cargo via a diacidic motif. *Mol Microbiol* **68**: 1535–1546.

Lin, J., Annoura, T., Sajid, M., Chevalley-Maurel, S., Ramesar, J., Klop, O., *et al.* (2011) A novel 'gene insertion/marker out' (GIMO) method for transgene expression and gene complementation in rodent malaria parasites. *PLoS One* **6**: e29289.

Lindner, S.E., Sartain, M.J., Hayes, K., Harupa, A., Moritz, R.L., Kappe, S.H.I., and Vaughan, A.M. (2014) Enzymes involved in plastid-targeted phosphatidic acid synthesis are essential for *Plasmodium yoelii* liver-stage development. *Mol Microbiol* **91**: 679–693.

Loureiro, J., Lilley, B.N., Spooner, E., Noriega, V., Tortorella, D., and Ploegh, H.L. (2006) Signal peptide peptidase is required for dislocation from the endoplasmic reticulum. *Nature* **441**: 894–897.

Matz, J.M., Goosmann, C., Brinkmann, V., Grützke, J., Ingmundson, A., Matuschewski, K., and Kooij, T.W.A. (2015) The *Plasmodium berghei* translocon of exported proteins reveals spatiotemporal dynamics of tubular extensions. *Sci Rep* **5**: 12532.

Menard, R., Tavares, J., Cockburn, I.A., Markus, M., Zavala, F., and Amino, R. (2013) Looking under the skin:

the first steps in malarial infection and immunity. *Nat Rev Microbiol* **11**: 701–712.

Mikolajczak, S.A., Jacobs-Lorena, V., MacKellar, D.C., Camargo, N., and Kappe, S.H.I. (2007) L-FABP is a critical host factor for successful malaria liver stage development. *Int J Parasitol* **37**: 483–489.

Parvanova, I., Epiphanio, S., Fauq, A., Golde, T.E., Prudêncio, M., and Mota, M.M. (2009) A small molecule inhibitor of signal peptide peptidase inhibits Plasmodium development in the liver and decreases malaria severity. *PLoS One* **4**: e5078.

Pattaradilokrat, S., Li, J., and Su, X. (2011) Protocol for production of a genetic cross of the rodent malaria parasites. *J Vis Exp* 5–10.

Pédelacq, J.D., Cabantous, S., Tran, T., Terwilliger, T.C., and Waldo, G.S. (2006) Engineering and characterization of a superfolder green fluorescent protein. *Nat Biotechnol* **24**: 79–88.

Phillips, M.J., and Voeltz, G.K. (2015) Structure and function of ER membrane contact sites with other organelles. *Nat Rev Mol Cell Biol* **17**: 1–14.

Prado, M., Eickel, N., De Niz, M., Heitmann, A., Agop-Nersesian, C., Wacker, R., *et al.* (2015) Long-term live imaging reveals cytosolic immune responses of host hepatocytes against plasmodium infection and parasite escape mechanisms. *Autophagy* **11**: 1561–1579.

Prasad, R., Atul, Kolla, V.K., Legac, J., Singhal, N., Navale, R., *et al.* (2013) Blocking *Plasmodium falciparum* development via dual inhibition of hemoglobin degradation and the ubiquitin proteasome system by MG132. *PLoS One* **8**: e73530.

Reimold, A.M., Iwakoshi, N.N., Manis, J., Vallabhajosyula, P., Szomolanyi-Tsuda, E., Gravallese, E.M., *et al.* (2001) Plasma cell differentiation requires the transcription factor XBP-1. *Nature* **412**: 300–307.

Sakaguchi, M., Miyazaki, N., Fujioka, H., Kaneko, O., and Murata, K. (2016) Three-dimensional analysis of morphological changes in the malaria parasite infected red blood cell by serial block-face scanning electron microscopy. *J Struct Biol* **193**: 162–171.

Schuck, S., Prinz, W.A., Thorn, K.S., Voss, C., and Walter, P. (2009) Membrane expansion alleviates endoplasmic reticulum stress independently of the unfolded protein response. *J Cell Biol* **187**: 525–536.

Sheffield, P., Garrard, S., and Derewenda, Z. (1999) Overcoming expression and purification problems of RhoGDI using a family of 'parallel' expression vectors. *Protein Expr Purif* **15**: 34–39.

Slavic, K., Delves, M.J., Prudêncio, M., Talman, A.M., Straschil, U., Derbyshire, E.T., *et al.* (2011) Use of a selective inhibitor to define the chemotherapeutic potential of the plasmodial hexose transporter in different stages of the parasite's life cycle. *Antimicrob Agents Chemother* **55**: 2824–2830.

Snapp, E.L., Hegde, R.S., Francolini, M., Lombardo, F., Colombo, S., Pedrazzini, E., *et al.* (2003) Formation of stacked ER cisternae by low affinity protein interactions. *J Cell Biol* **163**: 257–269.

Stanway, R., Graewe, S., Rennenberg, A., Helm, S., and Heussler, V.T. (2009) Highly efficient subcloning of rodent malaria parasites by injection of single merosomes or detached cells. *Nat Protoc* **4**: 1433–1439.

Stanway, R., Mueller, N., Zobiak, B., Graewe, S., Froehlke, U., Zessin, P.J.M., *et al.* (2011) Organelle segregation into Plasmodium liver stage merozoites. *Cell Microbiol* **13**: 1768–1782.

Striepen, B., Jordan, C.N., Reiff, S., and van Dooren, G.G. (2007) Building the perfect parasite: cell division in apicomplexa. *PLoS Pathog* **3**: e78.

Struck, N.S., de Souza Dias, S., Langer, C., Marti, M., Pearce, J.A., Cowman, A.F., and Gilberger, T.W. (2005) Re-defining the Golgi complex in *Plasmodium falciparum* using the novel Golgi marker PfGRASP. *J Cell Sci* **118**: 5603–5613.

Struck, N.S., Herrmann, S., Langer, C., Krueger, A., Foth, B.J., Engelberg, K., *et al.* (2008a) Plasmodium falciparum possesses two GRASP proteins that are differentially targeted to the Golgi complex via a higher- and lower-eukaryote-like mechanism. *J Cell Sci* **121**: 2123–2129.

Struck, N.S., Herrmann, S., Schmuck-Barkmann, I., de Souza Dias, S., Haase, S., Cabrera, A.L., *et al.* (2008b) Spatial dissection of the cis- and trans-Golgi compartments in the malaria parasite *Plasmodium falciparum*. *Mol Microbiol* **67**: 1320–1330.

Sturm, A., Graewe, S., Franke-Fayard, B., Retzlaff, S., Bolte, S., Roppenser, B., *et al.* (2009) Alteration of the parasite plasma membrane and the parasitophorous vacuole membrane during exo-erythrocytic development of malaria parasites. *Protist* **160**: 51–63.

Szul, T., and Sztul, E. (2011) COPII and COPI traffic at the ER-Golgi interface. *Physiology* **26**: 348–364.

Teixeira, J.E., and Huston, C.D. (2008) Evidence of a continuous endoplasmic reticulum in the protozoan parasite *Entamoeba histolytica*. *Eukaryot Cell* **7**: 1222–1226.

Thiberge, S., Blazquez, S., Baldacci, P., Renaud, O., Shorte, S., Ménard, R., and Amino, R. (2007) In vivo imaging of malaria parasites in the murine liver. *Nat Protoc* **2**: 1811–1818.

Voeltz, G.K., Rolls, M.M., and Rapoport, T.A. (2002) Structural organization of the endoplasmic reticulum. *EMBO Rep* **3**: 944–950.

Wang, M., and Kaufman, R.J. (2014) The impact of the endoplasmic reticulum protein-folding environment on cancer development. *Nat Rev Cancer* **14**: 581–597.

Westrate, L.M., Lee, J.E., Prinz, W.A., and Voeltz, G.K. (2015) Form follows function: the importance of endoplasmic reticulum shape. *Annu Rev Biochem* **84**: 791–811.

Wu, H., Ng, B.S.H., and Thibault, G. (2014) Endoplasmic reticulum stress response in yeast and humans. *Biosci Rep* **34**: 321–330.

Supporting information

Additional supporting information may be found in the online version of this article at the publisher's web-site.